Definition of a mutual reference shape based on information theory and active contours

S. Jehan-Besson[a], C. Tilmant[b], A. de Cesare[c], A. Lalande[d], A. Cochet[d], J. Cousty[e], J. Lebenberg[c], M. Lefort[c], P. Clarysse[f], R. Clouard[a,g], L. Najman[e], L. Sarry[h], F. Frouin[c], M. Garreau[i]

[a]*CNRS, UMR 6072 GREYC, F-14032 Caen, France*
[b]*CNRS UMR 6602 ; Université Blaise Pascal, Institut Pascal, Clermont-Ferrand, France*
[c]*Inserm U678 ; UPMC UMR_S 678, LIF, Paris, France*
[d]*CNRS UMR 6306, Université de Bourgogne, Le2I, Dijon, France*
[e]*Université Paris Est, UMR 8049, Laboratoire d'Informatique Gaspard Monge, France*
[f]*Université de Lyon, CREATIS ; CNRS UMR 5220 Inserm U1044 ; INSA-Lyon, Villeurbanne, France*
[g]*ENSICAEN, UMR 6072 GREYC, F-14050 Caen, France*
[h]*CNRS UMR 6284 ; Université d'Auvergne, ISIT, Clermont-Ferrand, France*
[i]*Inserm U1099 ; Université de Rennes 1, LTSI, Rennes, France*

Abstract

In this paper, we propose to consider the estimation of a reference shape from a set of different segmentation results using both active contours and information theory. The reference shape is then defined as the minimum of a criterion that benefits from both the mutual information and the joint entropy of the input segmentations. This energy criterion is here justified using similarities between information theory quantities and area measures, and presented in a continuous variational framework. This framework brings out some interesting evaluation measures such as the specificity and sensitivity. In order to solve this shape optimization problem, shape derivatives are computed for each term of the criterion and interpreted as an evolution equation of an active contour. A *mutual* shape is then estimated together with the sensitivity and specificity. Some synthetical examples allow us to cast the light on the difference between our mutual shape and an average shape. The applicability and robustness of our framework has also been tested for the evaluation of different segmentation methods of the left ventricular cavity from cardiac MRI.

Keywords: Active contours, segmentation evaluation, shape gradients, shape optimization, average shape, cardiac MRI.

1. Introduction

Constructing a reference shape from a set of different segmentation results is an important point when dealing with segmentation evaluation without knowing the gold standard. It can also be useful in order to combine different expert segmentations in a single reference shape. The reference shape must then take advantage of the information provided by each input shape while being robust to outliers. The estimation of such a reference shape can then be modeled using information theory (mutual information and joint entropy) through the definition of a shape optimization problem. In this paper, we propose to compute what we call a "mutual shape" using the framework of active contours and shape gradients. Our method is illustrated on a cardiac Magnetic Resonance Imaging (MRI) study and applied to the estimation of a reference shape of the left ventricular cavity, using the contours provided by six different algorithms.

As far as segmentation evaluation without gold standard is concerned, let us note that two main strategies have been classically adopted. The first one consists in choosing one parameter and in evaluating the performance level of each segmentation algorithm according to the relevance of this parameter within a selected database (e.g. in the domain of cardiac MRI, the left ventricular ejection fraction is the most important global physiological parameter depicting the myocardial contraction). Such an evaluation may be performed without a ground truth using some assumptions on the distribution of the chosen parameter (see for example [30, 40]). The second strategy consists in the estimation of a reference shape from all the segmentation entries. Each individual segmentation is then compared to the estimated reference contour using some quantitative measures (average distance to the reference contour, Hausdorff distance, Dice coefficient, specificity and sensitivity measures ...). We can say that this strategy corresponds to a verification step of the proposed algorithms accuracy, while in the former strategy, this is rather a validation step according to the user goal (e.g. ejection fraction). As far as the verification issue is concerned, the STAPLE algorithm (Simultaneous Truth and Performance Level Estimation) proposed by Warfield et al. [42] is now classically used in this difficult context. Their algorithm consists in one instance of the EM (Expectation Maximisation) algorithm where the true segmentation is estimated by maximizing the likelihood of the complete data. Their pixel-wise approach leads to the estimation of a reference shape simultaneously with the sensitivity and specificity of each input segmentation. From these measures, the

performance level of each input segmentation can be estimated and a classification of all the segmentation entries can be performed.

The algorithms proposed above in order to estimate a shape reference are local and treat each pixel independently. The MAP-STAPLE [7] is semi-local by using a small window or patch around the pixel. Moreover, the reference domain does not appear in the proposed model since it is defined only through the union of the selected pixels or through a thresholding of some features. Using such local or semi-local approaches, it appears difficult to introduce global information on the estimated shape (e.g information on the regularity of the contour or continuity of the labels within a given domain). In order to cope with these drawbacks, we propose to revisit the seminal work of Warfield [42] within a continuous optimization setting by considering such a shape estimation under the umbrella of shape optimisation tools [12] and deformable models [22]. Indeed, the computation of a reference shape can be advantageously modeled as the optimum of a well chosen energy criterion and estimated by a shape gradient descent that corresponds to the deformation of an active shape. Such an estimate is also closely related to the introduction of shapes similarity measures. For example, such shape optimization algorithms have already been proposed in order to compute shape averages [6, 38] or more recently median shapes [2] by minimising different shape metrics like the Hausdorff distance in [6] or the symmetric area difference between shapes in [38]. Some other approaches also take advantage of well-appropriated distances between level-set shapes (see for example [32]).

However, the shapes obtained using the previous variational algorithms cannot be considered as reference shapes especially in the case of outliers segmentation. One of the contributions of this paper is then to take advantage of the analogies between information theory and area measures in order to estimate what we call a “mutual shape”. We propose to maximize the mutual information between the n input segmentations while minimizing the joint entropy. Such a statistical criterion can be interpreted as a robust measure of the symmetric area difference. In this variational setting, we propose to add a classical regularization term based on the curvature of the deformable contour. Such a term is weighted using a regularization parameter that controls the smoothness of the obtained contour. The statistical model brings out both the sensitivity and specificity parameters and these parameters are estimated jointly with the reference mutual shape in similar to the STAPLE algorithm. However, the energy criterion is different from STAPLE and justified using analogies between information theory quantities and area measures. Moreover, the advantage of our formalism is to make explicitly appear the domain and the associated contour. Such a formalism may also be interesting

in order to add some geometrical or photometric priors directly in the criterion to minimize.

The proposed algorithm is first tested on synthetic examples showing the differences between a classic average variational shape based on a symmetric area minimization [38], a simple majority voting shape and the proposed mutual shape. It is also evaluated in order to classify the performance levels of different segmentation methods of the left ventricular cavity. The obtained mutual shape is compared with a classic average shape and with a reference shape drawn by an expert. The robustness of the estimation to some outliers is also tested for these real examples.

In section 2, our mathematical framework and the proposed criterion for the estimation of the mutual shape are both presented. The criterion is then estimated in a continuous framework and expressed using domain or contour integrals in section 3. Such a continuous criterion can then be derived using shape optimization tools in order to compute the mutual shape (see section 4). Experimental results on synthetic examples are detailed in section 5 and on MR images in section 6.

2. Problem statement

Let $\mathcal{U}$ be a class of domains (open regular bounded sets, i.e. $\mathcal{C}^2$) of $\mathbb{R}^d$ (with $d = 2$ or 3). In this paper theoretical results are stated for $d = 2$ or $d = 3$ but the experimental results are conducted on 2D-images. We denote by Ω_i an element of $\mathcal{U}$ of boundary $\partial\Omega_i$. We consider $\{\Omega_1, ..., \Omega_n\}$ a family of n shapes where each shape corresponds to the segmentation of the same unknown object O in a given image. The image domain is denoted by $\Omega \in \mathbb{R}^d$. Our aim is to compute a reference shape μ that can closely represent the true object O (Fig.1). We propose to define the problem through a statistical representation of shapes embedded in an information theory criterion. Let us first recall the main shape representation models and criteria proposed in the literature.

2.1. Shape representation

The computation of a reference shape is closely linked to the choice of a representation. An analytical representation may be used as in [23] where the authors propose a statistical study of shapes by representing them as a finite number of points. Some authors prefer to choose an implicit representation of shapes which avoids the parametrization step. For example, in [2, 5] shapes are represented us-

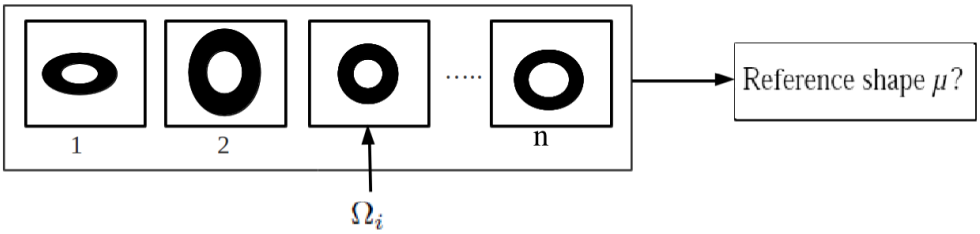

FIGURE 1: Diagram of the problem statement : evaluation of a reference shape μ from a set of n segmented shapes of the same object.

ing their characteristic function as follows :

$$d_i(\mathbf{x}) = \begin{cases} 1 & \text{if} \quad \mathbf{x} \in \Omega_i \\ 0 & \text{if} \quad \mathbf{x} \notin \Omega_i \end{cases} \tag{1}$$

where $\mathbf{x} \in \Omega$ is the location of the pixel within the image. We denote by $\overline{\Omega_i}$ the complementary shape of Ω_i in Ω with $\Omega_i \cup \overline{\Omega_i} = \Omega$.

One may also takes advantage of the distance function associated to each shape. In [32] the authors propose to perform a principal component analysis on shapes in order to provide a statistical shape prior. In the same vein, some statistical shape priors have been proposed by [10, 34] using this implicit representation.

More recently shapes have been represented using Legendre moments in order to define shape priors for segmentation using active contours [16, 17]. This representation can also be easily included in a variational setting [16, 17, 31].

We may also consider that each shape is a realization of a random variable. Such a representation has been introduced in [42] in order to evaluate a reference shape in a statistical framework, in [41] for the morphological exploration of shape spaces and statistics, and also in [19, 25] for image segmentation using information theory. In this paper, we take advantage of this statistical representation that appears to be well adapted to the definition of a statistical criterion. The shape is represented through a random variable D_i whose observation is the characteristic function d_i defined in (1). The reference shape μ is also represented through an unknown random variable T with the associated characteristic function $t(\mathbf{x}) = 1$ if $\mathbf{x} \in \mu$ and $t(\mathbf{x}) = 0$ if $\mathbf{x} \in \overline{\mu}$.

2.2. Definition of average shapes

We also need to formalize the unknown shape using the definition of a criterion to minimize. In the literature, average shapes are defined through the minimization

of the sum of the distances of the unknown shape μ to each shape Ω_i as follows :

$$\mu = \arg\min_{\mu^*} \sum_{i=1}^{n} d(\Omega_i, \mu^*) \tag{2}$$

Of course, the definition of the distance d is crucial and may lead to different results and average shapes. For example, an average shape can be computed by minimizing the area of the symmetric differences [38] using $d(\Omega_i, \mu) := |\Omega_i \triangle \mu|$ where $|.|$ stands for the cardinal of the considered domain. In a continuous optimization framework, the criterion to minimize according to μ can be expressed as follows :

$$SD(\mu) = \sum_{i=1}^{n} |\Omega_i \triangle \mu| = \sum_{i=1}^{n} \left(\int_{\mu} (1 - d_i(\mathbf{x}))d\mathbf{x} + \int_{\overline{\mu}} d_i(\mathbf{x})d\mathbf{x} \right) \tag{3}$$

In [5, 6], the authors prefer to introduce the Hausdorff distance to perform shape warping while in [2], the authors modify the previous criterion in order to compute *a median shape*.

In addition to the previous works, we can also cite [41] where the authors propose to explore shape spaces using mathematical morphology. The optimal shape is computed using a watershed performed on the squared sum of the distance functions or using a morphological computation of a median set. Another class of algorithms was proposed for the estimation of an unknown shape from multiple channels (color or multimodal segmentation). We can cite the work of Chan et al. [4] or the multimodal segmentation approaches proposed in [19, 24]. These works were not designed at first for segmentation evaluation but they are worth mentioning because they propose to treat the different channels in a single criterion (may also be useful for information fusion). Moreover in [19, 24], some information theory quantities are used. Our work is different especially due to the fact that we consider both the maximization of mutual information coupled with the minimization of joint entropies and the joint estimation of evaluation quantities (sensitivity and specificity measures).

2.3. Proposition of a criterion for the estimation of a mutual shape

Our goal is here to mutualize the information given by each segmentation to define a reference shape. Such a reference shape cannot be considered as a simple average shape. In this context, we propose to take advantage of the analogies between information measures (mutual information, joint entropy) and area measures.

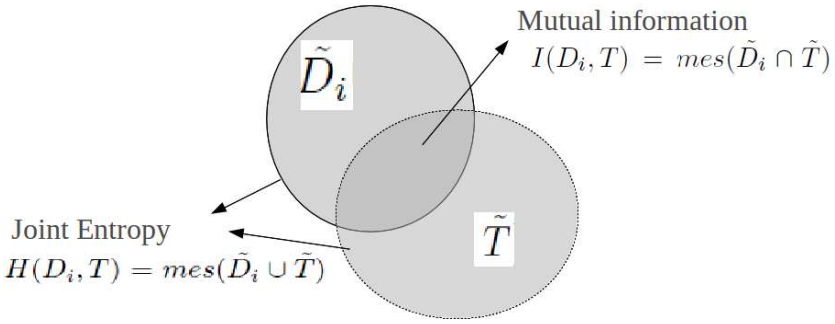

FIGURE 2: Mutual information and joint entropy as area measures

As previously mentioned, D_i represents the random variable associated with the characteristic function d_i of the shape Ω_i and T the random variable associated with the characteristic function t of the reference shape μ. Using these notations, $H(D_i,T)$ represents the joint entropy between the variables D_i and T, and $I(D_i,T)$ their mutual information. In [36, 43], it is shown that Shannon's information measures can be interpreted in terms of area measures as follows :

$$H(D_i,T) = \text{mes}(\tilde{D}_i \cup \tilde{T}) \quad \text{and} \quad I(D_i,T) = \text{mes}(\tilde{D}_i \cap \tilde{T}), \tag{4}$$

with $\tilde{X}$ the abstract set associated with the random variable X and mes a signed measure defined on an algebra of sets with values in $]-\infty,+\infty[$. The signed measure must satisfy $\text{mes}(\emptyset) = 0$ and $\text{mes}(\bigcup_{k=1}^{n} A_k) = \sum_{k=1}^{n} \text{mes}(A_k)$ for any sequence $\{A_k\}_{k=1}^{n}$ of disjoint sets. Each quantity can then be viewed as an operation on the sets (Fig.2). These properties will help us to better understand the role of each term chosen in our criterion.

When estimating a classic average shape using the criterion (3), one performs the minimization of the sum of the union of the shapes Ω_i with μ while maximizing the sum of the intersection between the same shapes. By analogy with this criterion, we prefer to minimize a measure of the union while maximizing a measure of the intersection through the use of information quantities. In other words, the sum of the joint entropies (union of sets) will be minimized while the sum of the mutual information quantities (intersection) will be maximized. In order to minimize a single criterion, we use the classic relation between mutual information and conditional entropy : $I(D_i,T) = H(D_i) - H(D_i/T)$. Since $H(D_i/T) \geq 0$ and $H(D_i)$ is independent of T, we will rather minimize $H(D_i,T)$. Due to all these

considerations and properties, we propose to minimize the following criterion :

$$E(T) = \sum_{i=1}^{n} (H(D_i, T) + H(D_i/T)) = JH(T) + MI(T), \tag{5}$$

where the sum of joint entropies is denoted by $JH(T) = \sum_{i=1}^{n} H(D_i, T)$ and the sum of conditional entropies by $MI(T) = \sum_{i=1}^{n} H(D_i/T)$.

Note that this criterion is implicitly based on the assumption that random variables D_i are considered as being independent. This assumption can be considered by the fact that the different Ω_i are generated from different and independent segmentation algorithms. In order to get rid of this assumption, one can think of maximizing the mutual information of joint random variables $I(D_1, D_2, .., D_n, T)$ but this criterion also leads to some computational issues that are difficult to solve.

3. Expression of the criterion in a continuous framework

In order to take advantage of the previous statistical criterion (5) within a continuous shape optimization framework, we propose to express the joint and conditional probability density functions according to the reference shape μ. This step is detailed in this section for both the mutual information and the joint entropy.

3.1. Maximization of mutual information (MI)

Here we try to express $MI(T) = \sum_{i=1}^{n} H(D_i/T)$ in a continuous setting according to the unknown shape μ. Denoting by t and d_i the observations of the random variables T and D_i, the conditional entropy of D_i knowing T can be written as follows :

$$H(D_i/T) = -\sum_{t \in \{0,1\}} \left[p(t) \sum_{d_i \in \{0,1\}} p(d_i/t) \log(p(d_i/t)) \right], \tag{6}$$

with $p(T = t) = p(t)$ and $p(D_i = d_i/T = t) = p(d_i/t)$.
The conditional probability $p(d_i = 1/t = 1)$ corresponds to the sensitivity parameter p_i (true positive fraction) :

$$p_i(\mu) = p(d_i = 1/t = 1) = \frac{1}{|\mu|} \int_{\mu} d_i(\mathbf{x}) d\mathbf{x}. \tag{7}$$

The conditional probability $p(d_i = 0/t = 0)$ corresponds to the specificity parameter q_i (true negative fraction) :

$$q_i(\mu) = p(d_i = 0/t = 0) = \frac{1}{|\overline{\mu}|} \int_{\overline{\mu}} (1 - d_i(\mathbf{x})) d\mathbf{x}. \tag{8}$$

In the rest of the paper, for the sake of simplicity, $p_i(\mu)$ is replaced by p_i and $q_i(\mu)$ by q_i. The random variable T takes the value 1 with a probability $p(t=1) = |\mu|/|\Omega|$ and 0 with a probability $p(t=0) = |\overline{\mu}|/|\Omega|$. The MI criterion can then be expressed according to μ :

$$MI(\mu) = -\sum_{i=1}^{n} \left[\frac{|\mu|}{|\Omega|}\left((1-p_i)\log(1-p_i) + p_i \log p_i\right) + \frac{|\overline{\mu}|}{|\Omega|}\left(q_i \log q_i + (1-q_i)\log(1-q_i)\right) \right]. \tag{9}$$

The parameters p_i and q_i depend explicitly on μ, which must be taken into account in the optimization process. Indeed if μ is updated in an iterative process, the parameters p_i and q_i must also be updated which implies a joint estimation of these quantities with the unknown mutual shape.

3.2. Minimization of joint entropy

Let us now express, according to μ and in a continuous setting, the sum of the joint entropies $JH(T) = \sum_{i=1}^{n} H(T, D_i)$. The following expression of the joint entropy is considered :

$$H(D_i, T) = -\sum_{t\in\{0,1\}} \sum_{d_i\in\{0,1\}} p(d_i,t)\log\left(p(d_i,t)\right), \tag{10}$$

with $p(D_i = d_i, T = t) = p(d_i, t)$.
The following estimates for the joint probabilities are then used ($a = 0$ or $a = 1$) :

$$p(d_i = a, t = 1) = \frac{1}{|\Omega|}\int_{\mu} \left((1-a)(1-d_i(\mathbf{x})) + a d_i(\mathbf{x})\right) d\mathbf{x}, \tag{11}$$

$$p(d_i = a, t = 0) = \frac{1}{|\Omega|}\int_{\overline{\mu}} \left((1-a)(1-d_i(\mathbf{x})) + a d_i(\mathbf{x})\right) d\mathbf{x}. \tag{12}$$

The criterion to minimize is now denoted by $JH(\mu)$ and can be written as follows :

$$JH(\mu) = -\frac{1}{|\Omega|}\sum_{i=1}^{n}\Big[\int_{\mu}\left((1-d_i(\mathbf{x}))\log\left(A_i(\mu)\right) + d_i(\mathbf{x})\log\left(B_i(\mu)\right)\right) d\mathbf{x} + \int_{\overline{\mu}}\left((1-d_i(\mathbf{x}))\log\left(A_i(\overline{\mu})\right) + d_i(\mathbf{x})\log\left(B_i(\overline{\mu})\right)\right) d\mathbf{x}\Big] + C, \tag{13}$$

$$\text{with} \quad A_i(\mu) = \int_{\mu}(1-d_i(\mathbf{x}))\, d\mathbf{x}, \quad A_i(\overline{\mu}) = \int_{\overline{\mu}}(1-d_i(\mathbf{x}))\, d\mathbf{x} \tag{14}$$

$$\text{and} \quad B_i(\mu) = \int_{\mu} d_i(\mathbf{x})\, d\mathbf{x}, \quad B_i(\overline{\mu}) = \int_{\overline{\mu}} d_i(\mathbf{x}) d\mathbf{x}. \tag{15}$$

The term C is equal to $n\log(\Omega)$ is independent from μ.

3.3. Continuous expression of the criterion

Using the two previous sections, we can express the global criterion to minimize according to μ as follows :

$$\begin{aligned} E(\mu) &= JH(\mu) + MI(\mu) \\ &= -\sum_{i=1}^{n} \Big[\frac{|\mu|}{|\Omega|} \left((1-p_i)\log(1-p_i) + p_i \log p_i\right) \\ &+ \frac{|\overline{\mu}|}{|\Omega|} \left(q_i \log q_i + (1-q_i)\log(1-q_i)\right) \\ &+ \frac{1}{|\Omega|} \int_{\mu} \left((1-d_i(\mathbf{x}))\log(A_i(\mu)) + d_i(\mathbf{x})\log(B_i(\mu))\right) d\mathbf{x} \\ &+ \frac{1}{|\Omega|} \int_{\overline{\mu}} \left((1-d_i(\mathbf{x}))\log(A_i(\overline{\mu})) + d_i(\mathbf{x})\log(B_i(\overline{\mu}))\right) d\mathbf{x} \Big] + C, \end{aligned} \tag{16}$$

where p_i, q_i, A_i and B_i are some quantities depending on the unknown shape μ expressed using integrals over μ.

In this given form, the minimization of such a criterion can be considered using active contours and shape gradients as detailed in the following section.

4. Optimization using shape gradients

In order to compute a local minimum of the criterion E, we propose to take advantage of the framework developed in [1] which is based on the shape optimization tools proposed in [12, Chap.8]. The main idea is to deform an initial curve (or surface) towards the boundaries of the region of interest. Formally, the contour then evolves according to the following Partial Differential Equation (PDE) :

$$\frac{\partial \Gamma(z,\tau)}{\partial \tau} = v(\mathbf{x},\mu)\mathbf{N}(\mathbf{x}) \tag{17}$$

where $\Gamma(z,\tau)$ is the evolving curve, z a parameter of the curve, τ the evolution parameter, $v(\mathbf{x},\mu)$ the amplitude of the velocity in $\mathbf{x} = \Gamma(z,\tau)$ directed along the normal of the curve $\mathbf{N}(\mathbf{x},\tau)$. The evolution equation and more particularly the

velocity v must be computed in order to make the contour evolve towards an optimum of the energy criterion (16). From an initial curve Γ_0 defined by the user, we will have $\lim_{\tau\to\infty}\Gamma(\tau)=\mu$ at convergence of the process.

The main issue lies in the computation of the velocity v in order to find the unknown shape μ at convergence. This term is deduced from the derivative of the criterion according to the shape. The method of derivation is explained in details in [1, 20] and is based on shape derivation principles developed formally in [12, 39]. For completeness, we recall some useful definitions and theorems and we then explain briefly how the evolution equation of an active contour can be deduced from the shape derivative. For each part of the criterion, the associated shape derivatives are computed with some explanations on the derivation.

4.1. Main mathematical tools

The following theorem is the central theorem for derivation of integral domains of the form $\int_\mu k(\mathbf{x},\mu)\,d\mathbf{x}$. It gives a general relation between the Eulerian derivative and the shape derivative for region-based terms.

Theorem 1 *Let Ω be a C^1 domain in $\mathbb{R}^n$ and $\mathbf{V}$ a C^1 vector field. Let k be a C^1 function. The functional $J(\mu)=\int_\mu k(\mathbf{x},\mu)\,d\mathbf{x}$ is differentiable and its Eulerian derivative in the direction of $\mathbf{V}$ is the following :*

$$< J'(\mu),\mathbf{V} >= \int_\mu k_s(\mathbf{x},\mu)\,d\mathbf{x} - \int_{\partial\mu} k(\mathbf{x},\mu)(\mathbf{V}\cdot\mathbf{N})\,d\mathbf{a} \tag{18}$$

where k_s is the shape derivative of k defined by $k_s(\mathbf{x},\mu)=\lim_{\tau\to 0}\frac{k(\mathbf{x},\mu(\tau))-k(\mathbf{x},\mu)}{\tau}$. The term $\mathbf{N}$ denotes the unit inward normal to $\partial\mu$ and $d\mathbf{a}$ its area element (in $\mathbb{R}^2$, we have $d\mathbf{a}=ds$ where s stands for the arc length).

The Eulerian derivative of J in the direction $\mathbf{V}$ is defined as

$$< J'(\mu),\mathbf{V} >= \lim_{\tau\to 0}\frac{J(\mu(\tau))-J(\mu)}{\tau}$$

if the limit exists, with $\mu(\tau)=T_\tau(\mathbf{V})(\mu)$ the transformation of μ through the vector field $\mathbf{V}$. The proof of the theorem can be found in [12, 20].

4.2. Methodology for the computation of the evolution equation

The following proposition gives us a way to compute the evolution equation of the active contour when the Eulerian derivative can be expressed as an integral over the boundary of the domain.

Proposition 1 *Let us consider that the shape derivative of the criterion $J(\mu)$ in the direction* $\mathbf{V}$ *may be written in the following way :*

$$< J'(\mu), \mathbf{V} >= -\int_{\partial\mu} v(\mathbf{x},\mu)(\mathbf{V}\cdot\mathbf{N})d\mathbf{a} \tag{19}$$

Interpreting this equation as the L^2 inner product on the space of velocities, the straightforward choice in order to minimize $J(\mu)$ consists in choosing $\mathbf{V} = v\mathbf{N}$ for the deformation. We can then deduce that, from an initial contour Γ_0, the boundary $\partial\mu$ can be found at convergence of the following evolution equation :

$$\frac{\partial\Gamma}{\partial\tau} = v(\mathbf{x},\tau)\mathbf{N} \tag{20}$$

with v the velocity of the curve and τ the evolution parameter.

The shape derivatives of the criteria $SD(\mu)$ (3), $MI(\mu)$ (9) and $JH(\mu)$ (13), can be written in the form (19) which allows us to find some geometrical PDEs of the form (20) for each criterion. The derivation is developed thereafter.

4.3. Shape derivatives

This paragraph details the computations of the shape derivatives of $SD(\mu)$ (3), $MI(\mu)$ (9) and $JH(\mu)$ (13).

4.3.1. Shape derivative for the criterion $SD(\mu)$

Theorem 2 *The shape derivative in the direction* $\mathbf{V}$ *of the functional $SD(\mu)$ defined in (3) is :*

$$< SD'(\mu), \mathbf{V} >= -\int_{\Gamma} \sum_{i=1}^{N} (1 - 2\,d_i(\mathbf{x}))(\mathbf{V}\cdot\mathbf{N})d\mathbf{a} \tag{21}$$

Corollary 1 *From Theorem* (1)*, the velocity that will drive an active contour towards a minimum of the criterion $SD(\mu)$ is reduced to :*

$$v_{SD} = \sum_{i=1}^{N} (1 - 2\,d_i(\mathbf{x})) \tag{22}$$

where v_{SD} is directed along $\mathbf{N}$*.*

4.3.2. Shape derivative for the criterion $MI(\mu)$

The computation of the shape derivative of $MI(\mu)$ is more complex because the functions inside the integrals depend on μ.

Theorem 3 *The shape derivative in the direction* $\mathbf{V}$ *of the functional* $MI(\mu)$ *defined in (9) is :*

$$< MI'(\mu), \mathbf{V} >= -\int_\Gamma \Big(\frac{1}{|\Omega|} \sum_{i=1}^{n} \Big[(1-d_i(\mathbf{x})) \log\left(\frac{q_i}{1-p_i}\right) \tag{23}$$

$$+ d_i(\mathbf{x}) \log\left(\frac{1-q_i}{p_i}\right) \Big] \Big) (\mathbf{V}\cdot\mathbf{N}) d\mathbf{a} \tag{24}$$

with $\mathbf{N}$ *the inward normal of the boundary of* μ *(denoted by* Γ*).*

Corollary 2 *From the Theorem* (1) *and* (3)*, the velocity that will drive an active contour towards a minimum of the criterion* $JH(\mu)$ *is then equal to :*

$$v_{MI} = \frac{1}{|\Omega|} \sum_{i=1}^{n} \Big[(1-d_i(\mathbf{x})) \log\left(\frac{q_i}{1-p_i}\right) + d_i(\mathbf{x}) \log\left(\frac{1-q_i}{p_i}\right) \Big] \tag{25}$$

where v_{MI} *is directed along* $\mathbf{N}$*.*

4.3.3. Shape derivative for the criterion $JH(\mu)$

Theorem 4 *The shape derivative in the direction* $\mathbf{V}$ *of the functional* $JH(\mu)$ *defined in (13) is :*

$$< JH'(\mu), \mathbf{V} >= -\int_\Gamma \Big(\frac{1}{|\Omega|} \sum_{i=1}^{n} \Big[d_i(\mathbf{x}) \log\left(\frac{B_i(\overline{\mu})}{B_i(\mu)}\right) \tag{26}$$

$$+ (1-d_i(\mathbf{x})) \log\left(\frac{A_i(\overline{\mu})}{A_i(\mu)}\right) \Big] \Big) (\mathbf{V}\cdot\mathbf{N}) d\mathbf{a}$$

where $\mathbf{N}$ *is the inward normal of the boundary of* μ *(denoted by* Γ*) and where the functionals* A_i *and* B_i *are given by equations* (14) *and* (15)*.*

Corollary 3 *From Theorem* (1) *and* (4)*, the velocity that will drive an active contour towards a minimum of the criterion* $JH(\mu)$ *takes the following expression :*

$$v_{JH} = \frac{1}{|\Omega|} \sum_{i=1}^{n} \Big[d_i(\mathbf{x}) \log\left(\frac{B_i(\overline{\mu})}{B_i(\mu)}\right) + (1-d_i(\mathbf{x})) \log\left(\frac{A_i(\overline{\mu})}{A_i(\mu)}\right) \Big] \tag{27}$$

where v_{JH} *is directed along* $\mathbf{N}$*.*

4.4. Global evolution equations for the different criteria

A standard regularization term is added in the criterion to minimize in order to favor smooth shapes :

$$Reg(\mu) = \int_{\partial\mu} ds.$$

This term corresponds to the minimization of the curve length. It is balanced with a positive coefficient λ in the energy criterion and leads to the following velocity in the evolution equation :

$$v_{Reg} = \kappa \tag{28}$$

where κ is the curvature of the contour $\Gamma(\tau)$.

Finally, we propose to define our mutual reference shape through the minimization of a global criterion called J_{IT} (Information Theoretic criterion) :

$$J_{IT}(\mu) = JH(\mu) + MI(\mu) + \lambda Reg(\mu). \tag{29}$$

In order to minimize this criterion, the following evolution equation is used :

$$\left(\frac{\partial\Gamma}{\partial\tau}\right)_{IT} = (v_{JH} + v_{MI} + \lambda v_{Reg})\,\mathbf{N} \tag{30}$$

where v_{MI}, v_{JH} and v_{Reg} are defined respectively in equations (25), (27) and (28). In the experimental results, the mutual reference shape is also compared to the classic average shape that corresponds to the minimization of the following criterion :

$$J_{SD}(\mu) = SD(\mu) + \lambda Reg(\mu). \tag{31}$$

In order to minimize this second criterion, the following evolution equation is applied :

$$\left(\frac{\partial\Gamma}{\partial\tau}\right)_{SD} = (v_{SD} + \lambda v_{Reg})\,\mathbf{N} \tag{32}$$

where v_{SD} and v_{Reg} are defined respectively in equations (22) and (28).

Note also that using this formalism, some other prior information (photometric or geometric) can be inserted by adding some additional velocities in the PDE. For example, we may take advantage of the tools developed in [3, 11, 17, 31, 34].

5. Experimental results on a synthetic example

The behaviour of our mutual shape estimation is tested on a synthetic example. We propose to compare the mutual shape with the classic average shape and with a simple majority voting. We also study the joint evolution of the sensitivity and specificity parameters.

5.1. Difference between a mutual shape and a classic average shape

In this section, the behaviour of such a mutual informative shape is illustrated by a synthetic example that highlights the difference between the mutual shape and a classic average shape. A test sequence consisting of different segmentations of a lozenge (Fig.3) was built. The first entry is the true segmentation mask, the other entries represent the segmentation of $1/4$ of the true lozenge (Fig.3(b)).

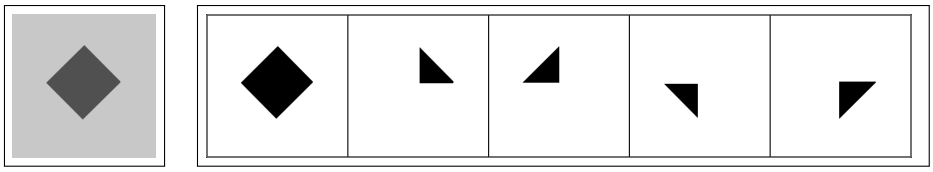

(a) (b)

FIGURE 3: The image to segment is given in (a) and the different segmentation entries (masks) for this image are given in (b).

When computing the average of the different characteristic functions using the formula : $\sum_{i=1}^{n} d_i/n$, we can remark (Fig.4(b)) that some masks share an intersection. Indeed the values of the average image belong to the interval $[0, 0.6]$. The value 0 corresponds to black points in Fig.4(a) and the value 0.6 corresponds to the white grey level in this image. We then binarize this average image I_A in an image named I_{AT} displayed in (Fig.4(b)). If $I_A(\mathbf{x}) \geq 0.5$ then $I_{AT} = 0$ (black points) and if $I_A(\mathbf{x}) < 0.5$ then $I_{AT} = 255$ (white points). This procedure gives us a simple majority voting procedure. The result is the black line inside the lozenge. The result obtained using this procedure is also dependent on the threshold parameter choice.

Then an active contour evolves according to the evolution equation of the mutual shape (30) and of the SD shape (32). The initial contour for the evolution is chosen as a circle including the lozenge (Fig.5(a) and Fig.6(a)). The mutual shape algorithm is able to recover the whole lozenge and is then different from a classic average shape (see Fig.5 and Fig.6). The curve evolves and segments the

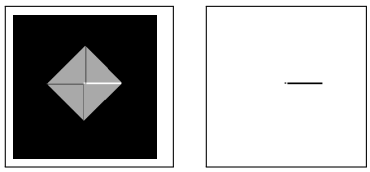

(a) (b)

FIGURE 4: The average image I_A (a) and the corresponding binarized average image I_{AT} (b) of the masks of the Fig.3(b) (simple majority voting procedure).

whole lozenge by an iterative process (images resulted from different iterations in Fig.5(b) and Fig.5)(c)). The final contour is given in Fig.5(d). The mutual shape is compared to a shape average computed using the minimization of the classic symmetrical difference (criterion J_{SD} with evolution equation (32)). The evolution is given in Fig.6. In this case, the final contour is similar to the result obtained by computing a binarized mean I_{AT} (Fig.4(b)) since it corresponds to a line due to the small overlap between masks 2 and 5. The same small value is taken for the regularization parameter λ in order to give an higher importance to the data term.

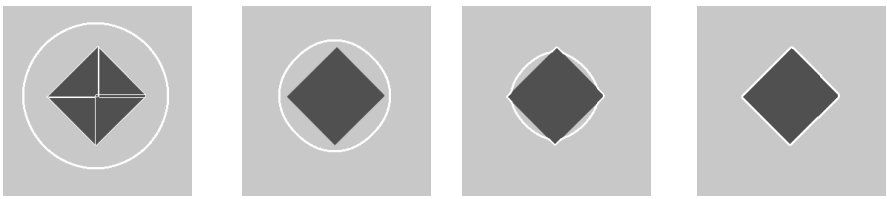

(a) Initial contour (b) It. 80 (c) It. 140 (d) Mutual shape

FIGURE 5: Evolution using the mutual shape (evolution equation (30) with $\lambda = 10$). In the first image (a), the initial contour is in white (circle) and the other white lines represent the boundaries of the different segmentation entries. Intermediate results obtained from 80 and 140 iterations are displayed in images (b) and (c) and the final estimated mutual shape in (d) (240 iterations).

5.2. Difference between the mutual shape and the union of the masks

An outlier (Fig.7(a)) was introduced in the initial sequence of masks in order to test the robustness of the mutual shape estimation. Indeed, our goal is to test that the mutual shape is also different to a simple union of the different masks. In Fig.7, the different steps of the evolution of the contour are displayed. The final contour (Fig.7(d)) fits the lozenge and excludes the outlier from the final contour.

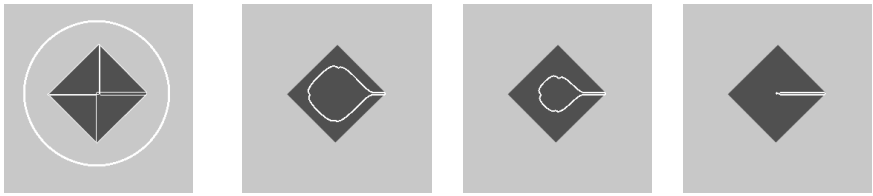

(a) Initial contour (b) It. 300 (c) It. 400 (d) SD shape

FIGURE 6: Evolution using the SD shape (evolution equation (32) with $\lambda = 10$). In the first image, the initial contour is in white (circle) and the other white lines represent the boundaries of the different segmentation entries. Intermediate results obtained from 300 and 400 iterations are displayed in images (b) and (c) and the final estimated SD shape in (d) (600 iterations).

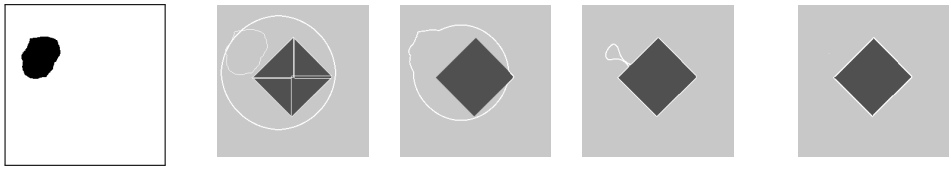

(a) Input outlier (b) Initial (c) It. 100 (d) It. 380 (e) Mutual shape

FIGURE 7: Introduction of an outlier (a) in the initial sequence of masks (Fig.3.a b) and estimation of the mutual shape (evolution equation (30) with $\lambda = 10$). In the image (b), the initial contour is in white and the other white contours and lines represent the different boundaries of the initial masks (the segmentation entries and the outlier).

5.3. Joint evolution of the sensitivity and specificity parameters

When the active contour evolves using the evolution equation (30), the parameters p_i and q_i are estimated jointly with the mutual shape as proposed in STAPLE [42]. The joint evolution of these parameters associated to each segmentation result are shown in Table 1. These results are obtained when considering the different entries displayed in the first row of this Table. According to the final values reported in Table 1, we can conclude that the best segmentation corresponds to the shape 1 with $p_1 = 1$ and $q_1 = 1$ and that the shape 6 is an outlier since the sensitivity coefficient is equal to 0. The other segmentations correspond to one quarter of the lozenge which leads to a sensitivity parameter around the value of 0.25. Note that the initial values of p_i and q_i are computed directly using the initial contour as an intial guess of the reference shape μ.

We can notice that the parameter q_i is less relevant. Indeed this parameter is estimated using the external domain ($\bar{\mu}$) and is then estimated using a higher

number of pixels. It should be normalized in order to be comparable to the p_i value. One solution consists in the selection of a smaller working area (a mask that includes the union of masks and that limits the size of the region outside this union in order to get two regions with a comparable size).

In order to give an idea of the computational cost, it takes around 5 s. to perform the estimation of the mutual shape for an image $256 * 256$ using an Intel Core i7 2.70GHz and a code written in C++ within the image processing library Pandore [1].

Iterations	mask 1	mask 2	mask 3	mask 4	mask 5	 mask 6
It. 0 (Fig. 7.b)	$p_1 = 0.35$ $q_1 = 1$	$p_2 = 0.09$ $q_2 = 1$	$p_3 = 0.09$ $q_3 = 1$	$p_4 = 0.08$ $q_4 = 1$	$p_5 = 0.09$ $q_5 = 1$	$p_6 = 0.15$ $q_6 = 1$
It. 100 (Fig. 7.c)	$p_1 = 0.60$ $q_1 = 1$	$p_2 = 0.15$ $q_2 = 1$	$p_3 = 0.15$ $q_3 = 1$	$p_4 = 0.13$ $q_4 = 1$	$p_5 = 0.16$ $q_5 = 1$	$p_6 = 0.27$ $q_6 = 1$
Final (Fig. 7.d)	$p_1 = 1$ $q_1 = 1$	$p_2 = 0.24$ $q_2 = 1$	$p_3 = 0.26$ $q_3 = 1$	$p_4 = 0.22$ $q_4 = 1$	$p_5 = 0.27$ $q_5 = 1$	$p_6 = 0$ $q_6 = 0.93$

TABLE 1: Joint evolution of the contour and of the sensitivity and specificity coefficients p_i and q_i for the all the segmentation entries (masks 1 to 6) corresponding to the evolution of the contour displayed in Fig.7 (initial contour, iteration 100 and final contour).

6. Application to the evaluation of different segmentation methods of the left ventricular cavity from cardiac MRI

The estimation of such a mutual shape is here tested for the unsupervised evaluation of segmentation methods of the left ventricular cavity from cardiac cine-MRI. It takes place in a larger project on medical segmentation evaluation first introduced in [26, 18] and developed thereafter in [21, 27, 29, 30]. To illustrate our method, one image is extracted from a series acquired with a SSFP sequence in a short axis orientation. The test carried out on this image can be used for all the images from all the series.

In order to compare a given shape Ω with a reference shape Ω_{ref}, we mainly use three quantitative values : the classic Dice coefficient (DC), the maximum and

1. available at https ://clouard.users.greyc.fr/Pandore/

the average distance to the reference contour (d_{max} and d_{mean}). The quantity DC [13] is a similarity measure between two sets that ranges into the interval $[0,1]$:

$$DC(\Omega,\Omega_{ref}) = \frac{2|\Omega \cap \Omega_{ref}|}{|\Omega| + |\Omega_{ref}|}. \tag{33}$$

This measure is equal to 1 when the two sets are equal and 0 when they are disjoints.
The distance between a point of the contour Γ to the contour Γ_{ref} is computed as follows :

$$d(\mathbf{y},\Gamma_{ref}) = \inf_{\mathbf{x}\in\Gamma_{ref}} (||\mathbf{y}-\mathbf{x}||). \tag{34}$$

From this previous definition, we can compute the maximum and the average distance (in pixels) using :

$$d_{max}(\Gamma,\Gamma_{ref}) = \max_{\mathbf{y}\in\Gamma} d(\mathbf{y},\Gamma_{ref}), \tag{35}$$

$$d_{mean}(\Gamma,\Gamma_{ref}) = \frac{1}{|\Gamma|}\sum_{\mathbf{y}\in\Gamma} d(\mathbf{y},\Gamma_{ref}). \tag{36}$$

where $|\Gamma|$ gives the number of pixels $\mathbf{y}\in\Gamma$.

6.1. Estimation of the mutual shape for one slice

The segmentation inputs correspond to the segmentation results obtained by different research teams [8, 9, 14, 15, 28, 31, 37] for a MRI slice of the 2009 MICCAI challenge database (SCN05, slice 4, time 20) [35] (Fig.8). The corresponding contours of the different entries of the algorithm are given in Fig.8. The expert contour is available for this slice and represented in Fig.8(g).

6.1.1. Comparison of the mutual shape with the expert contour and the SD shape

The mutual shape is estimated using the evolution equation (30) from the masks of the Fig.8. The initial contour is chosen near the contour of the masks union and the regularization parameter is fixed to the value 100.

The estimated mutual shape is shown in Fig.9(a) as well as the shape obtained using SD in Fig.9(c). The maximum distance to the expert contour (d_{max}) and the mean distance to the expert contour (d_{mean}) were calculated in order to validate the robustness of our algorithm. The mutual shape is nearer the expert contour in terms of distance. In Fig.9(b) and (d), the expert contour is drawn in white while the estimated shape is drawn in different colors according to the distance to

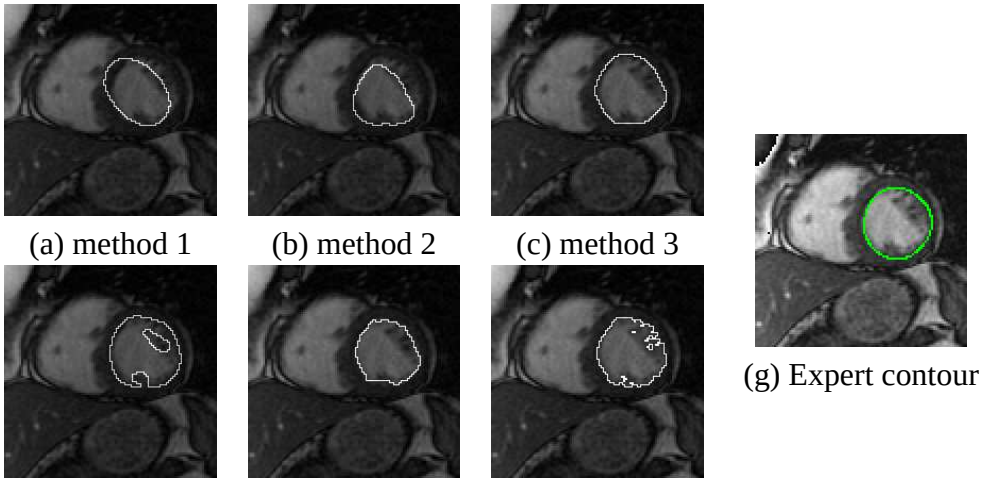

(a) method 1 (b) method 2 (c) method 3

(g) Expert contour

(d) method 4 (e) method 5 (f) method 6

FIGURE 8: The final contours of the six methods are given in (a),(b),(c),(d),(e),(f). These methods all aim to segment the left ventricular cavity from a MRI slice (SCN05, slice 4, time 20). The expert contour is also given in (g).

the expert contour. DC is equal to 0.89 for the mutual shape and to 0.87 for the SD shape using the same regularization parameter $\lambda = 100$. The influence of this parameter is developed in the next section.

6.1.2. Influence of the regularization parameter

The influence of the parameter λ that controls the weight of the regularization parameter was then tested.We report in Table 2 the different values of the three parameters d_{mean}, d_{max} and DC for the two shapes "mutual shape" and "SD shape" according to the regularization parameter λ. We also show the influence of this parameter on the different contours obtained for the mutual shape in Fig.10. In both cases, a value of λ around 100 may improve the evaluation coefficients DC, d_{mean} and d_{max}. This can be easily explained by the fact that the left ventricular cavity is a convex structure. Choosing a high value for λ may then help to provide such a convex shape. Reasonable values for the segmentation of this structure range into the interval $[100 - 300]$. The best value is probably around 100 for the mutual shape and 300 for the SD shape but there are very few differences when taking a regularization parameter into the interval $[100 - 300]$. When taking a higher value for λ, the regularization term takes a higher importance than the data term leading to an under-segmentation of the cavity.

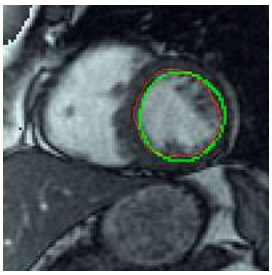

(a) mutual and expert shape (in red and green)

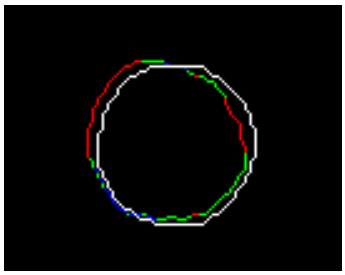

(b) distances to the expert for the mutual shape ($d_{mean} = 1.65, d_{max} = 3.35, DC = 0.89$)

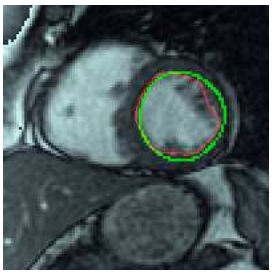

(c) SD and expert shape (in red and green)

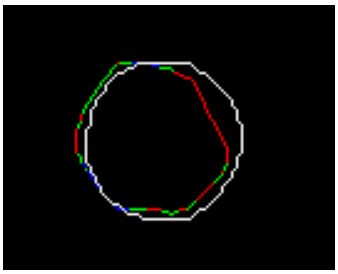

(d) distances to the expert for the SD shape ($d_{mean} = 1.80, d_{max} = 5.22, DC = 0.87$)

FIGURE 9: Qualitative and quantitative comparisons of the mutual shape ((a) and (b)) and the SD shape ((c) and (d)). In the images (a) and (c), the final contours are given in red and the expert contour in green ($\lambda = 100$)). In the images (b) and (d) the expert contour (in white) is superimposed with the final contour (the different colors correspond to the distance to the expert contour : the point x of the contour is in blue when $d(x) \leq 2$, in green when $2 < d(x) \leq 4$ and in red when $d(x) > 4$).

6.2. Robustness to outliers

In order to study the robustness, we introduce some outliers shapes represented in Fig.11. The outliers (1) and/or (2) and/or (3) were introduced to the initial sequence of masks (Fig.8). The variation of the chosen parameters (DC, d_{mean}, d_{max}) is then studied. The results are reported in Table 3 and compared to the ones obtained while estimating the reference shape using the classic symmetric difference (32). We remark that the quantitative parameters are quite stable when adding outliers to the initial sequence up to 3 added outliers which represent half of the number of initial masks. Using the SD shape, the coefficient is not as stable as with the mutual shape.

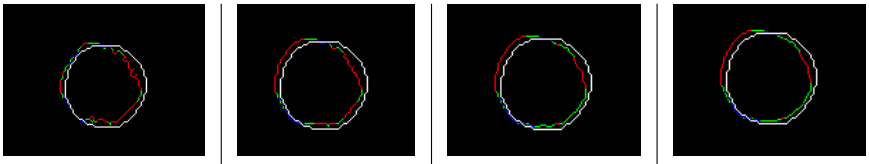

(a) $\lambda = 0$ $d_{mean} = 1.86$ $d_{max} = 5.00$ | (b) $\lambda = 10$ $d_{mean} = 1.86$ $d_{max} = 5.00$ | (c) $\lambda = 100$ $d_{mean} = 1.65$ $d_{max} = 3.35$ | (d) $\lambda = 300$ $d_{mean} = 1.66$ $d_{max} = 3.54$

FIGURE 10: Influence of the parameter λ on the final mutual shape. In the images (a), (b) and (c), the expert contour (in white) is surimposed with the final contour (in different colors according to the distance to the expert contour : the point x of the contour is in blue when $d(x) \leq 2$, in green when $2 < d(x) \leq 4$ and in red when $d(x) > 4$).

The evolution of the curve with both the mutual shape and the SD shape is displayed in Fig.12. The initial contour is chosen near to the union of the mask (choosing exactly the union can sometimes conduct to local minima due to the initial values of q_i that are all equal to 1).

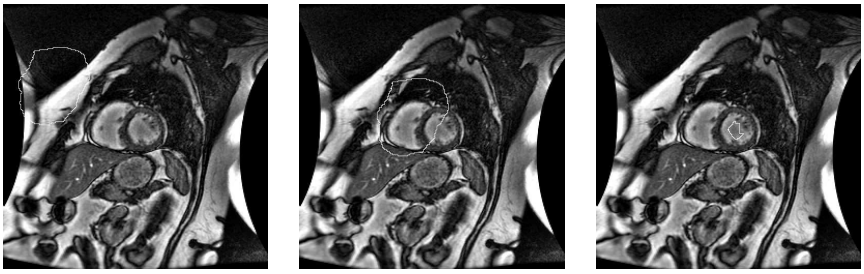

Outlier shape (1) Outlier shape (2) Outlier shape (3)

FIGURE 11: Contours of the different outliers.

6.3. Joint estimation of the sensitivity and specificity parameters

During the curve evolution, the parameters p_i and q_i are estimated jointly with the mutual shape and allow us to perform a classification of the performance level of each segmentation. According to the final values reported in Table 4, we can conclude that the best segmentation corresponds to shape 3 and that the shapes 1 and 2 have smaller sensitivity and specificity values. Such a classification seems to be visually coherent.

(a) Mutual shape					
λ	0	10	100	300	500
DC	0.885	0.884	0.887	0.886	0.861
d_{mean}	1.86	1.86	1.65	1.66	1.94
d_{max}	5.00	5.00	3.35	3.54	4.72

(b) SD shape					
λ	0	10	100	300	500
DC	0.867	0.869	0.873	0.873	0.870
d_{mean}	1.98	1.87	1.80	1.78	1.84
d_{max}	5.83	5.83	5.22	5.00	5.22

TABLE 2: Influence of the regularization parameter λ on the final shape for both the mutual shape (a) and the SD shape (b).

When computing p_i and q_i note that it works better when the regions inside and outside the contour have a comparable number of pixels. Indeed adding a pixel in each region will then lead to a comparable change in the computation of p_i and q_i. In this work, in order to deal with this issue, a region of interest outside the contour is defined at the beginning of the evolution. However, a region of interest that evolves during the curve evolution could be a better solution but needs further investigation and probably the framework introduced in [33].

7. Conclusion

In this work, we propose a continuous optimization framework for the STAPLE algorithm using a different criterion to minimize that comes from information theory. We take advantage of information theory quantities such as the mutual information and joint entropy. We propose a new criterion based on the minimization of a robust area difference that can be expressed using mutual information and joint entropy. We search for an unknown reference shape that minimizes the sum of joint entropies while maximizing the sum of mutual information between each entry shape and the unknown reference shape. The optimization is performed using active contours by computing a shape gradient and the associated evolution equation. Shape derivatives are detailed for the given criterion but also for a classic area difference minimization. Our theoretical formalism is valid for 2D slices or 3D images. Some experimental results are provided in 2D images on both synthetic and real cardiac cine-MRI images. The robustness of such an estimate is

(a) Quantitative results with the mutual shape (evolution equation (30)**)**						
	Outlier shape number(s)					
Comparison meas.	none	1	2	1+2	3	1+2+3
DC	0.887	0.887	0.884	0.884	0.887	0.870
d_{mean}	1.65	1.65	1.65	1.69	1.65	1.84
d_{max}	3.35	3.35	3.35	3.35	3.35	5.03

(b) Quantitative results with the symmetric difference (evolution equation (32)**)**						
	Outlier shape number(s)					
Comparison meas.	none	1	2	1+2	3	1+2+3
DC	0.873	0.860	0.860	0.797	0.871	0.788
d_{mean}	1.80	1.96	2.00	2.67	1.82	2.75
d_{max}	5.22	5.41	5.66	8.94	5.66	9.39

TABLE 3: Comparison of the final contour with the expert contour in presence of outliers.

Classification using p_i and q_i						
i	1	2	3	4	5	6
q_i	0.93	0.97	0.97	0.91	1	0.99
p_i	0.77	0.68	0.98	0.85	0.83	0.92

TABLE 4: Specificity and specificity parameters p_i and q_i for the different segmentation methods of the left ventricular cavity displayed in Fig.8 (without considering the outliers).

tested by adding some outliers to the input sequence. We show that the mutual shape acts differently and is more robust to outliers than other conventional approaches.

As far as perpectives are concerned, one of the main issues may concern the choice of the main objective for the evaluation. Indeed in our case, in cardiac imaging, the goal was to estimate the volume of the cardiac cavity. In this case, adding a prior term on the shape of the endocardium may be valuable. If the objective is different, some other prior shapes may be added (such as the homogeneity of the inside region for example). Our mathematical framework seems well adapted for this purpose since other information may be easily added in the criterion to minimize. Our work in progress concerns also the comparison of our method to STAPLE algorithms and will be extended to a larger database of real cardiac cine-MRI images.

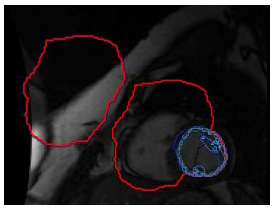

(a) Initial contour (red)

(b) iteration 900

(c) Mutual final shape

(d) SD final shape

FIGURE 12: Evolution of the curve for the mutual shape and the SD shape. The initial contour is given in red (a) surimposed on the contours of the different segmentation entries (blue). For the mutual shape, the iteration 900 is shown in (b) while the final contour given in (c). In order to compare, we show the final contour for the SD (symmetrical difference) criterion.

Acknowledgements

This work took place in a larger project on segmentation evaluation named MediEval supported by the GdR 2647 Stic Santé (CNRS-INSERM).

Annexes

We give here some proofs in order to detail the computation of shape derivatives.

Proof of theorem 2

Proof : The criterion (3) can be divided into two parts : the first one depends on the domain μ and is denoted by $SD_1(\mu)$ with $SD_1 = \int_\mu (1 - d_i(\mathbf{x}))d\mathbf{x}$ while the second one depends on the complementary domain of μ and is denoted by $SD_2(\mu)$ with $SD_2 = \int_{\overline{\mu}} d_i(\mathbf{x})d\mathbf{x}$.

From Theorem (1) and using the fact that the derivative k_s is equal to 0 (d_i is independent of μ), the following equation can be obtained :

$$< SD_1'(\mu), \mathbf{V} >= -\int_{\partial\mu} k(\mathbf{x},\mu)(\mathbf{V}\cdot\mathbf{N})\, d\mathbf{a}$$

with $k(\mathbf{x},\mu) = 1 - d_i(\mathbf{x})$.

In order to derive SD_2, the same theorem is applied :

$$< SD_2'(\mu), \mathbf{V} >= -\int_{\partial\overline{\mu}} d_i(\mathbf{x})(\mathbf{V}\cdot\mathbf{N}_2)\, d\mathbf{a}$$

with $\mathbf{N}_2$ the inward normal of the boundary of $\overline{\mu}$.
Since μ and $\overline{\mu}$ share the same boundary Γ with opposite normal vectors (i.e. $\mathbf{N} = -\mathbf{N}_2$), we find the derivative given in (21).

■

Proof of theorem 3

Proof : Using Theorem (1), the shape derivatives of p_i and q_i are equal to :

$$< p_i', V >= \frac{1}{|\mu|}\int_\Gamma (p_i - d_i(\mathbf{x}))(\mathbf{V}\cdot\mathbf{N})d\mathbf{a},$$

$$< q_i', V >= \frac{1}{|\overline{\mu}|}\int_\Gamma (1 - d_i(\mathbf{x}) - q_i)(\mathbf{V}\cdot\mathbf{N})d\mathbf{a}.$$

Let us denote $K_i(\mu) = |\mu| f(p_i)$ with $f(p_i) = (1-p_i)\log(1-p_i) + p_i\log(p_i)$, we can deduce :

$$_< K_i'(\mu), \mathbf{V} >= -\int_\Gamma f(p_i) + (p_i - d_i) f'(p_i)(\mathbf{V}\cdot\mathbf{N})d\mathbf{a}.$$

with $f'(p_i) = \log\frac{p_i}{1-p_i}$ the classic derivative of f according to the variable p_i. After simplifications, we get :

$$< K_i'(\mu), \mathbf{V} >= -\int_\Gamma (d_i \log p_i + (1-d_i)\log(1-p_i))(\mathbf{V}\cdot\mathbf{N})d\mathbf{a}.$$

In the same manner, $E_i(\mu) = |\overline{\mu}| f(q_i)$ with $f(q_i) = (1-q_i)\log(1-q_i) + q_i\log q_i$ and then :

$$< E_i'(\mu), \mathbf{V} >= \int_\Gamma ((1-d_i(\mathbf{x}))\log q_i + d_i(\mathbf{x})\log(1-q_i))(\mathbf{V}\cdot\mathbf{N})d\mathbf{a}.$$

By adding the different terms, we find the final shape derivative.

■

Proof of theorem 4

Proof : As with the theorem 2, the criterion is separated in different terms, such that $JH(\mu) = -\frac{1}{|\Omega|}\sum_{i=1}^{n}(JH_1^i(\mu) + JH_2^i(\mu)) + C$ with :

$$JH_1^i(\mu) = \log A_i(\mu)\int_\mu (1-d_i(\mathbf{x}))\,d\mathbf{x} + \log B_i(\mu)\int_\mu d_i(\mathbf{x})\,d\mathbf{x},$$
$$JH_2^i(\mu) = \log A_i(\overline{\mu})\int_{\overline{\mu}} (1-d_i(\mathbf{x}))\,d\mathbf{x} + \log B_i(\overline{\mu})\int_{\overline{\mu}} d_i(\mathbf{x})\,d\mathbf{x}.$$

The term C denotes a constant independent of μ.
The shape derivative of $A_i(\mu)$ lead to $< A_i'(\mu), \mathbf{V} >= -\int_\Gamma (1-d_i(x))(\mathbf{V}\cdot\mathbf{N})d\mathbf{a}$ and respectively $< B_i'(\mu), \mathbf{V} >= -\int_\Gamma d_i(x)(\mathbf{V}\cdot\mathbf{N})d\mathbf{a}$.

The classic theorems for the derivation of products and functions can be applied to derive JH_1^i, which leads to :

$$\begin{aligned} < (JH_1^i)'(\mu), \mathbf{V} >= \quad - \quad & \log A_i(\mu)\int_\Gamma (1-d_i)(\mathbf{V}\cdot\mathbf{N})d\mathbf{a} + \frac{< A_i'(\mu), \mathbf{V} >}{A_i(\mu)}\int_\mu (1-d_i)\,d\mathbf{x} \\ & - \log B_i(\mu)\int_\Gamma d_i(\mathbf{V}\cdot\mathbf{N})d\mathbf{a} + \frac{< B_i'(\mu), \mathbf{V} >}{B_i(\mu)}\int_\mu d_i\,d\mathbf{x}. \end{aligned}$$

Replacing the shape derivative of $A_i(\mu)$ and $B_i(\mu)$ by their expressions in the above formula, we find :

$$< (JH_1^i)'(\mu), \mathbf{V} >= -\int_\Gamma \left((1-d_i)\log A_i(\mu) + d_i \log B_i(\mu) + 1\right)(\mathbf{V}\cdot\mathbf{N})d\mathbf{a}.$$

In a similar manner, using the fact that the inward normal of the moving boundary of $\overline{\mu}$ is equal to $-\mathbf{N}$, we find :

$$< (JH_2^i)'(\mu), \mathbf{V} >= \int_\Gamma \left((1-d_i(\mathbf{x}))\log A_i(\overline{\mu}) + d_i(\mathbf{x}) \log B_i(\overline{\mu}) + 1\right)(\mathbf{V}\cdot\mathbf{N})d\mathbf{a}.$$

By adding the two derivatives, the shape derivative of $JH(\mu)$ is finally obtained.

■

Références

[1] G. Aubert, M. Barlaud, O. Faugeras, and S. Jehan-Besson. Image segmentation using active contours : Calculus of variations or shape gradients. SIAM Applied Mathematics, 63 :2128–2154, 2003.

[2] B. Berkels, G. Linkmann, and M. Rumpf. An SL(2) invariant shape median. Journal of Mathematical Imaging and Vision, 37(2) :85–97, 2010.

[3] T. F. Chan and L. A. Vese. Active contour without edges. IEEE Image Processing, 10 :266–277, 2001.

[4] T.F. Chan, B.Y. Sandberg, and L.A. Vese. Active contours without edges for vector-valued images. Journal of Visual Communication and Image Representation, 11 :130–141, 2000.

[5] G. Charpiat, O. Faugeras, and R. Keriven. Shape metrics, warping and statistics. In International Conference on Image Processing, volume 2, pages II–627–630, 2003.

[6] G. Charpiat, O. Faugeras, and R. Keriven. Approximations of shape metrics and application to shape warping and empirical shape statistics. Foundations of Computational Mathematics, 5 :1–58, 2005.

[7] O. Commowick, A. Akhondi-Asl, and S.K. Warfield. Estimating a reference standard segmentation with spatially varying performance parameters. IEEE Transactions on Medical Imaging, 31(8) :1593–1606, august 2012.

[8] C. Constantinides, R. El Berbari, A. de Cesare, Y. Chenoune, E. Roullot, A. Herment, E. Mousseaux, and F. Frouin. Development and evaluation of an algorithm for the automated segmentation of the left and right ventricles on cine MRI. IRBM (Ingénierie et Recherche Biomédicale), 30(4) :188–191, 2009.

[9] J. Cousty, L. Najman, M. Couprie, S. Clément-Guinaudeau, T. Goissen, and J. Garot. Segmentation of 4D cardiac MRI : automated method based on spatio-temporal watershed cuts. Image and Vision Computing, 28(8) :1229–1243, 2010.

[10] D. Cremers, T. Kohlberger, and C. Schnörr. Shape statistics in kernel space for variational image segmentation. Pattern Recognition, 36 :1929–1943, 2003.

[11] D. Cremers, M. Rousson, and R. Deriche. A review of statistical approaches to level set segmentation : integrating color, texture, motion and shape. International Journal of Computer Vision, 72 :195–215, 2007.

[12] M.C. Delfour and J.P. Zolésio. Shapes and Geometries : Metrics, Analysis, Differential Calculus, and Optimization. Advances in design and control. Society for Industrial and Applied Mathematics (SIAM), 2001.

[13] L.R. Dice. Measures of the amount of ecologic association between species. Ecology, 26 :297–302, Jul. 1945.

[14] J. Fleureau, M. Garreau, D. Boumier, and A. Hernandez. 3D multi-object segmentation of cardiac MSCT imaging by using a multi-agent approach. In IEEE Engineering in Medicine and Biology Society, pages 6004–7, 2007.

[15] J. Fleureau, M. Garreau, A. Simon, R. Hachemani, and D. Boulmier. Assessment of global cardiac function in MSCT imaging using fuzzy connectedness segmentation. In Computers in Cardiology, pages 725–728, 2008.

[16] A. Foulonneau, P. Charbonnier, and F. Heitz. Geometric shape priors for region-based active contours. In IEEE International Conference on Image Processing, pages 413–416, 2003.

[17] A. Foulonneau, P. Charbonnier, and F. Heitz. Affine-invariant geometric shape priors for region-based active contours. IEEE Transactions on Pattern Analysis and Machine Intelligence, 28(8) :1352–1357, 2006.

[18] F. Frouin, M. Garreau, I. Buvat, C. Casta, C. Constantinides, J. Cousty, A. Cochet, S. Jehan-Besson, C. Tilmant, M. Lefort, L. Najman, L. Sarry, P. Clarysse, A. de Cesare, and A. Lalande. Méthodologie pour comparer différentes méthodes d'extraction de biomarqueurs sans méthode de référence. application à la segmentation du ventricule gauche en irm cardiaque pour estimer la fraction d'éjection. In Colloque RITS (Recherche en Imagerie et Technologies pour la Santé), Rennes, 2011.

[19] A. Herbulot, S. Jehan-Besson, S. Duffner, M. Barlaud, and G. Aubert. Segmentation of vectorial image features using shape gradients and information measures. Journal of Mathematical Imaging and Vision, 25(3) :365–386, 2006.

[20] S. Jehan-Besson, M. Barlaud, and G. Aubert. DREAM^{2}S : Deformable regions driven by an eulerian accurate minimization method for image and video segmentation. International Journal of Computer Vision, 53(1) :45–70, 2003.

[21] S. Jehan-Besson, C. Tilmant, A. De Cesare, F. Frouin, L. Najman, A. Lalande, L. Sarry, C. Casta, P. Clarysse, C. Constantidinès, J. Cousty, M. Lefort, A. Cochet, and M. Garreau. Estimation d'une forme mutuelle pour l'évaluation de la segmentation en imagerie cardiaque. GRETSI - Traitement du Signal et des Images, 2011.

[22] M. Kass, A. Witkin, and D. Terzopoulos. Snakes : Active contour models. International Journal of Computer Vision, 1 :321–332, 1988.

[23] D.G. Kendall. Shape manifolds, procrustean metrics, and complex projective spaces. Bull. London Math. Soc., 16(2) :81–121, 1984.

[24] J. Kim, J.W. Fisher, A. Yezzi, M. Cetin, and A.S. Willsky. Nonparametric methods for image segmentation using information theory and curve evolution. In IEEE International Conference on Image Processing, pages 797–800, 2002.

[25] J. Kim, J. Fisher III, A. Yezzi Jr., M. Cetin, and A. Willsky. Nonparametric methods for image segmentation using information theory and curve evolution. In IEEE International Conference on Image Processing, pages 1522–4880, September 2002.

[26] A. Kissi, C. Tilmant, A. De Cesare, A. Comte, L. Najman, A. Lalande, P. Clarysse, M. Garreau, L. Sarry, and F. Frouin. Initiative multicentrique pour une plateforme d'évaluation en imagerie cardiaque. In Colloque RITS (Recherche en Imagerie et Technologies pour la Santé), Lille, 2009.

[27] A. Lalande, J. Lebenberg, I. Buvat, P. Clarysse, C. Casta, A. Cochet, C. Constantinidès, J. Cousty, A. de Cesare, S. Jehan-Besson, M. Lefort L. Najman, E. Roullot, L. Sarry, C. Tilmant, M. Garreau, and F. Frouin. A reference free approach for the comparative evaluation of eight segmentation methods for the estimation of the left ventricular ejection fraction in cardiac mri. In Scientific Meeting of the European Society for Magnetic Resonance in Medicine and Biology (ESMRMB), page 658, 2012.

[28] A. Lalande, N. Salve, A. Comte, M.-C. Jaulent, L. Legrand, P.M. Walker, Y. Cottin, J.E. Wolf, and F. Brunotte. Left ventricular ejection fraction calculation from automatically selected and processed diastolic and systolic frames in short axis cine-MRI. Journal of Cardiovascular Magnetic Resonance, 6(4) :817–827, 2004.

[29] J. Lebenberg, I. Buvat, M. Garreau, C. Casta, C. Constantinidès, J. Cousty, A. Cochet, S. Jehan-Besson, C. Tilmant, M. Lefort, E. Roullot, L. Najman, P. Clarysse, A. de Cesare, A. Lalande, and F. Frouin. Comparison of different segmentation approaches without using gold standard. application to the estimation of the left ventricle ejection fraction from cardiac cine mri sequences. In IEEE Engineering in Medicine and Biology Society, pages 2663–2666, 2011.

[30] J. Lebenberg, I. Buvat, A. Lalande, P. Clarysse, C. Casta, A. Cochet, C. Constantinidès, J. Cousty, A. de Cesare, S. Jehan-Besson, M. Lefort, L. Najman, E. Roullot, L. Sarry, C. Tilmant, M. Garreau, and F. Frouin. Non supervised ranking of different segmentation approaches : application to the estimation of the left ventricular ejection fraction from cardiac cine MRI sequences. IEEE Transactions on Medical Imaging, 31(8) :1651–1660, 2012.

[31] F. Lecellier, S. Jehan-Besson, J. Fadili, G. Aubert, M. Revenu, and E. Saloux. Region-based active contours with noise and shape priors. In IEEE International Conference on Image Processing, volume 1, pages 1649–1652, 2006.

[32] M. Leventon, E. Grimson, and O. Faugeras. Statistical shape influence in geodesic active contours. In IEEE International Conference on Image Processing, pages 316–323, 2000.

[33] J. Mille. Narrow band region-based active contours and surfaces for 2D and 3D segmentation. Computer Vision and Image Understanding, 113(9) :946–965, 2009.

[34] N. Paragios. A level set approach for shape-driven segmentation and tracking of the left ventricle. IEEE Transactions on Medical Imaging, 22(6) :773–776, june 2003.

[35] P. Radau, Y. Lu, K. Connelly, G. Paul, A.J. Dick, and G.A. Wright. Evaluation framework for algorithm segmenting short axis cardiac MRI. The MIDAS Journal-Cardiac MR Left Ventricle Segmentation Challenge, 2009.

[36] F. M. Reza. An Introduction to Information Theory, pages 106–108. McGraw-Hill, 1994.

[37] J. Schaerer, C. Casta, J. Pousin, and P. Clarysse. A dynamic elastic model for segmentation and tracking of the heart in MR image sequences. Medical Image Analysis, 14(6) :738–749, 2010.

[38] S. Soatto and A.J. Yezzi. Deformotion : Deforming motion, shape average and the joint registration and segmentation of images. International Journal of Computer Vision, 53 :153–167, 2002.

[39] J. Sokolowski and J.-P. Zolésio. Introduction to shape optimization. Shape sensitivity analysis., volume 16 of Springer Series in Computational Mathematics. Springer-Verlag, Berlin, 1992.

[40] M. Soret, J. Alaoui, P.M. Koulibaly, J. Darcourt, and I. Buvat. Accuracy of partial volume effect correction in clinical molecular imaging of dopamine transporter using spect. Nuclear Instruments and Methods in Physics Research, 571 :173–176, 2007.

[41] S. Velasco-Forero and J. Angulo. Statistical shape modeling using morphological representations. In IEEE International Conference on Image Processing, pages 3537–3540, 2010.

[42] S.K. Warfield, K. H. Zou, and W. M. Wells III. Simultaneous truth and performance level estimation (STAPLE) : an algorithm for the validation of image segmentation. IEEE Transactions on Medical Imaging, 23(7) :903–921, 2004.

[43] R. W. Yeung. A new outlook on shannon's information measures. IEEE Transactions on Information Theory, 37(3) :466–474, 1991.